HHS Public Access

Author manuscript

*Nat Methods*. Author manuscript; available in PMC 2019 May 30.

Published in final edited form as:

*Nat Methods*. 2018 December ; 15(12): 1098–1107. doi:10.1038/s41592-018-0215-8.

# An Explant Technique for High-Resolution Imaging and Manipulation of Mycobacterial Granulomas

**Mark R. Cronan**[1,*], **Molly A. Matty**[1], **Allison F. Rosenberg**[1], **Landry Blanc**[3], **Charlie J. Pyle**[1], **Scott T. Espenschied**[1], **John F. Rawls**[1], **Véronique Dartois**[3,4], and **David M. Tobin**[1,2,*]

[1]Department of Molecular Genetics and Microbiology, Duke University School of Medicine, Durham, North Carolina, USA

[2]Department of Immunology, Duke University School of Medicine, Durham, North Carolina, USA

[3]Public Health Research Institute, New Jersey Medical School, Rutgers, The State University of New Jersey, Newark, New Jersey, USA

[4]Department of Medicine, New Jersey Medical School, Rutgers, The State University of New Jersey, Newark, New Jersey, USA

## Abstract

A central and critical structure in tuberculosis, the mycobacterial granuloma consists of highly organized immune cells, including macrophages that drive granuloma formation through a characteristic epithelioid transformation. Difficulties in imaging within intact animals as well as the inherent caveats of *in vitro* assembly models have severely limited the study and experimental manipulation of mature granulomas. Here we describe a new *ex vivo* granuloma culture technique, wherein mature, fully organized granulomas are microdissected and maintained in three-dimensional culture. This approach, in which granulomas retain key bacterial and host characteristics, enables high-resolution microscopy of granuloma macrophage dynamics, including epithelioid macrophage motility and granuloma consolidation. Through mass spectrometry, we find active production of key phosphotidylinositol species identified previously in human granulomas. We describe a method to transfect isolated granulomas, enabling genetic manipulation. In addition, we provide proof-of-concept for host-directed small molecule screens, identifying PKC signaling as an important regulator of granuloma macrophage organization.



[*]Correspondence: D.M.T. (david.tobin@duke.edu) or M.R.C. (mark.cronan@duke.edu).

Contributions

M.R.C. and A.F.R. conceived of the approach and initiated the project. M.R.C., A.F.R. and M.A.M. developed the protocol and performed the experiments. M.A.M. developed the protocol for light sheet microscopy of granulomas. L.B. and V.D. designed and performed the mass spectrometry experiments and prepared associated figures. C.J.P. designed the lux expressing *M. marinum* strain and performed validation experiments. S.T.E. and J.F.R. conceived and performed cytospin experiments. M.R.C., M.A.M., A.F.R. and D.M.T. designed the experiments and analyzed the data. M.R.C. and D.M.T. wrote the manuscript with input from all authors.

Data availability statement

Data generated during the study is available on request from the authors.

Competing Interests

The authors declare no competing interests.

## Introduction

Infection with *Mycobacterium tuberculosis* (*Mtb*), the causative agent of tuberculosis, orchestrates the formation of an organized aggregate of host immune cells called the granuloma[1, 2]. Granulomas are constructed from both infected and uninfected host immune cells, particularly macrophages. The macrophages of the granuloma undergo substantial morphological transitions, called epithelioid transformation, characterized by cell-cell interdigitation, a flat, spread morphology, and broad induction of epithelial markers within macrophages[1–4]. Beyond macrophages, the granuloma contains other immune cell types, including neutrophils, monocytes, dendritic cells, and T and B cells[1, 2, 5, 6]. As the infection proceeds, cell death within the granuloma can result in the formation of a central core of necrotic cell debris in which many of the mycobacteria reside[1, 2]. Thus, the granuloma serves as a central site of interaction between the host immune system and pathogenic mycobacteria[1, 2].

Studies of granuloma formation and organization historically focused on histological analyses of tissues from animal models or human patients. The use of fixed tissue in these assays led to the notion that the granuloma is a static host structure, a view that has been challenged by recent findings illustrating the granuloma's dynamic nature[1, 7–9]. These granuloma dynamics can be host beneficial. For instance, monocyte departure from the granuloma is crucial for antigen delivery to the lymph node and underlies antigen presentation and development of an adaptive immune response[10, 11]. However, granuloma cellular dynamics can also be host detrimental. Departure of mycobacteria-containing macrophages or dendritic cells leads to mycobacterial dissemination[8, 12]. Granulomas undergo larger scale rearrangement as well, undergoing expansion, contraction, and even consolidation with neighboring granulomas over the course of infection[9, 13].

To date, the study of granuloma dynamics has been hampered by the difficulty of imaging the granuloma within a live host. Longitudinal imaging with PET/CT and intravital imaging have been used to circumvent these issues[9, 13–17]. Each technique, however, has limitations. PET/CT enables long-term imaging of granuloma dynamics[9, 13, 14], but provides images of moderate resolution and can be cost-prohibitive. Intravital imaging enables high resolution imaging of tuberculous granulomas[15, 17]. However, the invasive surgery and accompanying anaesthesia required for intravital microscopy limits this technique to shorter-term studies.

To circumvent these issues, cell culture models of granuloma formation have been developed using human PBMCs infected with *Mtb in vitro*[18–21]. This approach allows longitudinal imaging of spontaneously assembling granulomas *in vitro* that manifest attributes associated with *Mtb* granulomas *in vivo*, including macrophage aggregation and central necrosis[18–21]. However, in the absence of the complete set of morphological cues present *in vivo*, these *in vitro* assembled structures fail to undergo the complete spectrum of changes associated with the *Mtb* granuloma.

The zebrafish-*M. marinum* model has emerged as a particularly useful model to study the *in vivo* dynamics of mycobacterial granuloma formation[22]. *M. marinum*, one of the closest relatives of *Mtb*, forms granulomas in zebrafish that closely resemble human tuberculous

granulomas, including the development of a necrotic core, and induction of specific epithelial markers that mediate granuloma organization [4, 22–24]. Imaging of early granuloma formation within optically transparent larval zebrafish enabled new insights into granuloma dynamics[7, 8, 22]. However, larval zebrafish studies are restricted to the less organized early granulomas, as larvae do not survive long-term infection and fail to form the fully mature granulomas seen in infected adults[22, 24]. The mature, necrotic granulomas that form in adult zebrafish most closely resemble the necrotic granulomas seen in human disease[24–26]. However, adult zebrafish are optically opaque, making live imaging challenging.

We sought a method for high-resolution imaging and manipulation of organized granulomas. We previously demonstrated that granulomas could be dissected from adult zebrafish[4]. Here, we use multidimensional culture techniques to enable week-long *ex vivo* culture of granulomas isolated from infected animals. We term this technique Myco-GEM for Mycobacterial Granuloma Explant Model. The Myco-GEM approach allows culture of granulomas *ex vivo* for at least seven days, enabling longer-term imaging of cellular and bacterial dynamics within fully organized granulomas by epifluorescent, confocal, and light-sheet microscopy techniques. In Myco-GEM culture, granulomas retained the morphology and characteristic inflammatory markers observed *in vivo*. Myco-GEM enables visualization of macrophage movement within the granuloma and during consolidation of granulomas *ex vivo*, demonstrating substantial cell rearrangement even within the epithelioid layer of a mature granuloma. We generated genetic approaches to manipulate cultured granulomas and demonstrate the suitability of Myco-GEM for chemical and genetic screening approaches.

## Results

### Mycobacterial granulomas can be cultured *ex vivo*

Using our previously described granuloma dissection technique[4], we found that *M. marinum*-infected adult zebrafish provide 20–100 granulomas each, providing diverse endpoint assays. We reasoned that we could culture these granulomas *ex vivo*, enabling high-resolution imaging of cellular and mycobacterial dynamics within organized granulomas. We initially attempted to culture granulomas on tissue culture treated plastic wells. The cells of the granuloma survived but granuloma morphology was lost due to cells attaching to the tissue culture treated surface (Supplementary Fig. 1a). We tried suspending granulomas in low-melt agarose to prevent attachment to tissue culture plastic. However, this resulted in rapid death of granuloma cells (Supplementary Fig. 1b). We then turned to three-dimensional (3D) culture techniques, embedding granulomas within Matrigel, reasoning that ECM anchorage would facilitate survival of granulomas while avoiding the morphological deformation seen on plastic. Matrigel-embedded granulomas retained viability and native organization, while enabling the visualization of cell movements within the granuloma (Supplementary Fig. 1c, Supplementary Video 1).

To optimize granuloma culture, we tested a range of distinct 3D and 2.5D conditions. In 2.5D culture, granulomas are cultured on solidified ECM overlaid by a dilute solution of ECM in growth media. We found that 2.5D culture conditions were sufficient to maintain the morphology of granulomas by phase contrast microscopy for at least 6–7 days (Fig. 1a). Hematoxylin and eosin staining remains the most definitive method by which to assess

granuloma morphology. We stained paraffin sections of granulomas cultured for 6 days in 2.5D with hematoxylin and eosin and found that these granulomas still morphologically resemble granulomas from infected zebrafish, retaining the characteristic central necrotic core and epithelioid macrophages of the granuloma (Supplementary Fig. 1d).

To assess the viability of granuloma cells during 2.5D culture, we dissociated newly dissected granulomas and six-day cultured granulomas, stained with LIVE/DEAD dye and analyzed by flow cytometry. We found that the ratio of live to dead cells was similar between freshly dissected and cultured granulomas, with the majority of the cells retaining viability throughout culture (Fig. 1b). These results demonstrated that 2.5D culture could maintain granuloma morphology and viability. The dilute top layer of ECM used in 2.5D culture enabled the manipulation of granulomas either physically or through addition of exogenous compounds to the upper media layer. The 2.5D culture model, which we term Myco-GEM, provided a compromise between maintenance of granuloma structure, survival, and accessibility for experimental manipulation (Fig. 1c).

## Dissected granulomas retain the cellular heterogeneity observed *in vivo*

The macrophage is the defining cell type of the granuloma, but granulomas contain other immune cell types including neutrophils, monocytes, dendritic cells and T and B cells[1, 2, 5, 6]. To investigate the complement of cell types within dissected granulomas, we dissociated granulomas, concentrated cells by cytospin, and stained with Wright-Giemsa stain. In dissected granulomas, the majority of cells were macrophages and monocytes, consistent with a central role for the macrophage in the granuloma. We also identified populations of neutrophils, dendritic cells and lymphocytes within the dissected granulomas (Fig. 1d). Using CLARITY tissue clearing and antibody staining, we found that neutrophils within the dissected granulomas were predominantly localized to the margins of the granuloma, consistent with previous findings in zebrafish and human patient samples (Supplementary Fig. 2a, Supplementary Video 2)[4, 5]. Thus, granulomas isolated for Myco-GEM retain the diverse immune cell types observed *in vivo*.

The granuloma is characterized by cellular heterogeneity in inflammatory state[2]. We next assessed inflammatory heterogeneity in granulomas isolated for Myco-GEM. TNF is a crucial regulator of bacterial restriction that is highly expressed in animal models of mycobacterial infection[27–29]. We isolated granulomas from TNF transcriptional reporter zebrafish, *TgBAC(tnfa:gfp)*$^{pd1028}$ (*tnfa:gfp*)[30] infected with *M. marinum* and analyzed TNF transcriptional induction by flow cytometry. Consistent with previous findings in animal models[26–29], we found that dissected granulomas from *tnfa:gfp* animals had robust induction of TNF, but individual cells from the granuloma displayed substantial heterogeneity in TNF transcriptional induction (Fig. 1e). Inflammatory state also affects cellular reactive oxygen species (ROS) levels in macrophages and other immune cell types[31]. Interrogation of intracellular ROS levels by CellROX staining of dissociated granuloma populations demonstrated considerable heterogeneity in ROS levels within granuloma cells (Fig 1f). These findings demonstrate that dissected granulomas retain the heterogeneous inflammatory state observed in granulomas *in vivo* [2, 5].

### Granulomas cultured in Myco-GEM conditions retain *in vivo* characteristics

We used fluorescent mycobacterial strains to assess whether Myco-GEM conditions maintained mycobacterial viability and growth. Mycobacteria within the granuloma grew throughout Myco-GEM culturing, indicating that culture conditions maintain mycobacterial viability (Fig. 2a). *In vivo*, mycobacteria are frequently constrained within the granuloma's necrotic core[1, 2]. During Myco-GEM, bacteria occupied a central structure apparent in phase contrast images (Fig. 2a). Nuclear staining of CLARITY-cleared tissue demonstrated that these regions of high bacterial burden were devoid of nuclear staining, consistent with bacterial residence within the necrotic core (Supplementary Fig. 2b, Supplementary Video 3).

Previous work has demonstrated that mycobacteria *in vivo* are under cellular stress from host defense processes including free radical production, pH stress, and hypoxia[2, 32–34]. We assessed whether mycobacteria in Myco-GEM remain under cellular stress. We used *M. marinum* harboring the stress-responsive dosRS reporter plasmid *hspX'::GFP, smyc'::mCherry*[32] to assess bacterial physiological state. This reporter results in constitutive expression of mCherry, while *hspX*-driven GFP expression is induced by bacterial stress. Consistent with *in vivo* data[32], freshly dissected granulomas from animals infected with *M. marinum(hspX'::GFP, smyc'::mCherry)* contained dual GFP-and mCherry-positive mycobacteria, indicative of mycobacterial stress (Supplementary Fig. 3). This state was retained throughout *ex vivo* culture (Supplementary Fig. 3).

We next probed metabolic activity of macrophages within the granuloma. $^{13}$C glucose was incorporated into Myco-GEM growth media to trace the products of glycolysis in granulomas. In human and rabbit granulomas, elevated levels of arachidonic acid and arachidonic acid-containing lipid species have been described and are detectable by mass spectrometry from granuloma extracts[35]. Similarly, we found that granulomas in Myco-GEM incorporated $^{13}$C label into the glycerol moiety of arachidonic acid-containing phosphatidylinositols through at least four days of continuous culture (Supplementary Fig. 4a,4c,4d). Metabolic activity of cultured granulomas was retained throughout culture; we observed similar $^{13}$C incorporation in granulomas shifted into $^{13}$C containing media starting 4 days after plating (Supplementary Fig. 4b).

We previously described an epithelialization event in zebrafish and human granulomas in which macrophages form intra-macrophage adherens junctions[4]. To assess whether this host program remained intact in Myco-GEM cultured granulomas, we isolated granulomas from animals in which a fluorescently tagged plakoglobin (*Gt(jupa-citrine)*$^{ct520a}$, referred to as plakoglobin-citrine)[4] labels adherens junctions. We found that adherens junctions were formed between the cells of the granuloma and these junctions persisted throughout Myco-GEM culture (Fig. 2b). Plakoglobin can be recruited to adherens junctions formed by both epithelial and non-epithelial cadherins as well as desmosomal cadherins[36]. To further interrogate granuloma epithelialization, we engineered a new zebrafish line, (*cdh1-tdtomato*)$^{xt18}$ in which endogenous E-cadherin was tagged with tdTomato fluorescent protein by CRISPR-mediated knock-in. Similar to observations in plakoglobin-citrine animals, granulomas from cdh1-tdTomato knock-in animals had an organized network of E-cadherin positive adherens junctions surrounding the necrotic core (Supplementary Fig. 5a).

This network persisted throughout at least 5 days of culture, suggesting that the molecular architecture of the granuloma was maintained during *ex vivo* culture (Supplementary Fig. 5a,b).

Although we were able to image adherens junction formation by spinning disk confocal microscopy, light scattering by the intact granuloma tissue limited the depth of imaging (Supplementary Fig 6a). To visualize adherens junctions deeper within cultured granulomas, we identified conditions for lightsheet imaging of *ex vivo* cultured granulomas. Using lightsheet microscopy, we examined the dynamics of adherens junctions deep within the granuloma for more than 8 hours of continuous imaging (Supplementary Fig. 6b, Supplementary Fig. 7a). This approach could be applied to granulomas post-culture as well; we were able to extract granulomas grown as long as 7 days in Myco-GEM conditions and subsequently image them via light sheet microscopy (Supplementary Fig. 7b). These results demonstrate that the Myco-GEM technique can be combined with light sheet imaging to enable high-resolution imaging deep within the granuloma.

To determine if the inflammatory heterogeneity we described in dissected granulomas was maintained throughout Myco-GEM culturing, we used microscopy to longitudinally monitor TNF induction throughout culture in granulomas from *tnfa:gfp* animals. We observed considerable heterogeneity in TNF induction which persisted throughout *ex vivo* granuloma culture (Supplementary Fig. 8). Taken together with our previous findings, these results demonstrate that Myco-GEM serves as a useful surrogate for the granuloma *in vivo*, retaining the characteristic inflammatory heterogeneity seen in mycobacterial infection in animals[2, 5].

## Myco-GEM enables visualization of granuloma dynamics

During longitudinal studies, we observed substantial cell movement by phase contrast but could not track individual cells by phase contrast alone. To follow individual granuloma macrophages, we crossed the macrophage-specific Cre line *Tg*(*mfap4:icre-p2a-tomato*)$^{xt8}$ to the reporter line, *Tg*(*ubb:loxp-tagbfp2-stop-loxp-tomato*)$^{xt7}$[4, 37]. We selected *Tg(mfap4:icre-p2a-tomato; ubb:loxp-tagbfp2-stop-loxp-tomato)* (denoted macrophage lineage tracing hereafter) animals with only limited rearrangement to track individual cells. Cell tracking revealed that macrophages moved substantially within the granuloma (Fig. 3 and Supplementary Video 4). This movement was not simply treadmilling of macrophages toward the necrotic core; individual macrophages were observed to move towards, away from, and also perpendicularly to the core (Fig. 3 and Supplementary Video 4). These results demonstrate that the macrophages of the granuloma dynamically rearrange within the structure rather than remaining in a fixed position within the granuloma.

Granulomas can undergo larger scale reorganization during infection. Through genetic approaches and PET/CT imaging, consolidation of neighboring granulomas has been observed *in vivo*[9, 38]. Neither of these techniques, however, has enabled dissection of the consolidation process at a cellular level. To model consolidation within the Myco-GEM model, we positioned two granulomas in contact with each other. We followed individual cell and bacterial populations by combining differentially labeled granulomas. One granuloma ubiquitously expressed tomato fluorescent protein (*Tg(ubb:tomato)*$^{xt23}$) and was

infected with cerulean- expressing *M. marinum* and a second was unlabeled and infected with wasabi expressing *M. marinum*. Upon contact, the granulomas rapidly (~20–30 min) attached to one another and started to enmesh (Fig. 4a,b, Supplementary Video 5). By one day post-plating, the granuloma structures began to merge and cells from the *Tg(ubb:tomato)* granuloma were found in the unlabeled granuloma (Fig. 4a-e). This consolidation process was largely complete by 4–5 days post plating, with *Tg(ubb:tomato)* granuloma cells spread throughout the merged granulomas (Fig. 4f,g, Supplementary Video 5). Despite consolidation of granuloma cell populations, we did not observe fusion between the necrotic cores or transfer of bacteria during the time frame of our experiment. In total, these results demonstrate that granulomas undergo consolidation *ex vivo*, which we can visualize with cellular resolution.

## Genetic and chemical interrogation of cultured granulomas

Direct genetic perturbation of cultured granulomas would greatly expand the experimental possibilities of the Myco-GEM approach. We were able to identify conditions in which the granuloma could be transfected with exogenous RNAs (Fig. 5a). Transfection of granulomas with RNA encoding tdTomato fluorescent protein followed by culture enabled longitudinal observation of transfected cells (Fig 5b). Transfection of tdTomato RNA was not deleterious, as cells retained viability for at least 4 days post-transfection and could be seen moving within the granuloma, similar to our observations in lineage tracing experiments (Fig. 5b, Supplementary Video 6). These results establish a method to genetically perturb the cells within the granuloma, enabling future genetic screens within granulomas *ex vivo*.

*In vivo* efficacy of antimycobacterials often does not match reported *in vitro* minimum inhibitory concentrations (MICs), in part due to the granuloma and its constituent cells acting as barriers for drug access to mycobacteria within[39]. Thus we reasoned that the additional three-dimensional context offered by the Myco-GEM model would more accurately model the efficacy of antimycobacterial therapies *in vivo*. As proof of principle we used Myco-GEM to test a range of concentrations of established antibiotics. To enhance Myco-GEM throughput, we generated a luminescent strain of *M. marinum* by expressing the *lux* operon[40], enabling longitudinal monitoring of bacterial burden in 96-well format by plate reader. Treatment of granulomas with high concentrations of established TB drugs led to a loss of bacterial luminescence that correlated with CFU numbers from individual granulomas (Supplementary Fig. 9a,b). We used this luminescent strain to test a group of first-line and second-line drugs each at five distinct concentrations on cultured granulomas in 96-well format. We found that there were substantive differences in the minimum dose required to inhibit mycobacterial growth in Myco-GEM compared to established MIC values in broth culture (Supplementary Table 1)[41, 42]. Drugs such as rifampicin and ethambutol showed inhibition at concentrations near their MIC values, while others, such as isoniazid and streptomycin required doses in large excess of their MICs. These results suggested that Myco-GEM captures additional cellular context that may better reflect mycobacterial drug susceptibility patterns in vivo.

We also assessed whether Myco-GEM could be used for chemical genetic screening approaches. We previously described an apical-basal polarity pathway induced in

mycobacterial granulomas in conjunction with epithelialization pathways[4]. Based on these data, we focused on the atypical PKCs (aPKC), PKCι and PKCζ, which are required for apical-basal polarity in epithelial cells[43, 44]. We asked whether Gö6983, a broad-spectrum inhibitor of PKC isoforms, could alter epithelialization of cultured granulomas. Longitudinal analysis of Gö6983-treated granulomas by lightsheet microscopy demonstrated that Gö6983 treatment rapidly drove disassembly of adherens junctions within the granuloma (Fig. 6a, b, Supplementary Video 7,8). These results suggest that PKC activity is required for maintenance of adherens junction formation within the granulomas and epithelialization. More broadly, in conjunction with the bacterial and host markers we have previously described, these findings indicate that Myco-GEM may be used with chemical genetic approaches to interrogate diverse bacterial and host outcomes.

## Discussion

Here we have developed a method to culture mycobacterial granulomas *ex vivo,* which allows unprecedented visual access to and experimental manipulation of intact, organized granulomas. We find that granulomas maintained under our *ex vivo* culture methods survived for one week in our culture conditions and retained their native morphology and granuloma-specific gene expression programs. Maintenance of native morphology within the *ex vivo* granuloma cultures required the use of extracellular matrix. Integrins are known to be important for tissue morphology and polarity in a number of tissue types[45]. The requirement for ECM in granuloma maintenance suggests that integrin engagement may be crucial for patterning of this bacterially driven host immune structure as well.

The cultured granulomas recapitulate and maintain known features of human TB granulomas, including the diverse cellular composition, inflammatory heterogeneity, epithelioid morphology and the expression and localization of proteins involved in adherens junctions. We also find conservation of lipid species, as cultured granulomas actively produce specific arachidonic acid-containing phosphotidylinositol species present in human and macaque granulomas[35]. Arachidonic acid-derived eicosanoids have been implicated in controlling the host response to mycobacterial infection in a range of animal species and humans[46–49].

Considerable inflammatory heterogeneity has emerged as a conserved feature of granulomas in humans and models such as macaques that form well-organized granulomas[2, 5]. We found that the cells of the granuloma exhibited variation in both *tnfa* transcriptional induction and cellular ROS levels. Elevated levels of TNF and ROS are associated with classically activated M1 type macrophages[31]. Thus the varied levels of ROS and TNF induction that we see throughout the granuloma is likely consistent with observations in humans, macaques and rabbits that both M1 and M2 macrophages persist within the granuloma[5, 50].

Imaging of macrophages within cultured granulomas demonstrated substantial movement of granuloma macrophages. These macrophages moved in all directions and frequently modulated their shape and cellular processes. Previous studies using intravital microscopy of liver granulomas in mice found that macrophages exhibited only limited movement within the granuloma[15, 17]. However, the difficulty of intravital imaging in mice limited these

previous experiments to imaging sessions of only ~1 hour in duration[15, 17]. In our experiments, there was minimal movement of individual macrophages over this timeframe, and the movement of macrophages only became apparent over the longer time durations possible with the *ex vivo* technique. Thus our findings are consistent with previous intravital imaging studies wherein macrophages within the granuloma move, but at substantially slower rates than observed during macrophage directional migration within tissues[51].

By physically manipulating granulomas cultured *ex vivo* we were able to drive the consolidation of granulomas in culture. Bacterial genetic approaches and PET-CT imaging have demonstrated that consolidation between granulomas occurs in about 10% of granulomas[9, 38]. Here, using *ex vivo* granuloma culture techniques, we found that, upon contact, the granulomas rapidly adhered to one another, an adhesion event that rapidly became irreversible. The macrophages of the granuloma express classical epithelial markers[4], thus adhesion may be driven by the interaction in trans of epithelial adhesion molecules such as E-cadherin at the point of contact between granulomas.

During later stages of granuloma consolidation, the cells of the granulomas, which began to admix within hours of granuloma contact, appeared to be completely interspersed by four to five days after contact. Recent findings have characterized considerable heterogeneity within individual granulomas in morphology, cell types and gene expression[2]. The ready admixing of cells between two consolidating granulomas raises the question of whether the cells from the individual granulomas retain their unique characteristics or if the cells of both granulomas adopt a uniform character during consolidation.

Despite the consolidation between the cells of the granuloma, we did not observe necrotic core fusion or bacterial mixing, indicating that necrotic core consolidation occurred slowly if at all. Large, consolidated clusters of granulomas, called multifocal granulomas, have long been noted by pathologists. Barcoding experiments found that multifocal granulomas arise most frequently from local spread of bacteria to form secondary granulomas followed by consolidation of these granulomas[9, 38]. However, a subset of multifocal granulomas occur through consolidation between granulomas formed by distinct bacterial populations[9, 38]. Our data supports the idea that distinct necrotic foci may persist within these consolidated granulomas.

We demonstrate that the Myco-GEM model can be used as a platform to genetically interrogate granuloma structure by transfection of RNA. The population of cells transfected within the granuloma is restricted, likely due to the limited surface accessibility of the cells of the granuloma. However, this approach will enable the interrogation of host genes that act within the granuloma in a cell-autonomous fashion.

Treatment of Myco-GEM cultured granulomas with established anti-mycobacterial compounds demonstrated that the granulomatous context limited the efficacy of established therapies. There was considerable divergence in the concentration of each drug relative to the MIC required *in vitro* for effective reduction in bacterial burden. When considered relative to the *in vitro* MICs[41, 42], the efficacy of the drugs agree with previous studies characterizing the relative accumulation of chemotherapeutics within macrophages[52–57]. For

instance, in our assay, drugs known to accumulate at higher levels in macrophages like bedaquiline or ethambutol outperformed those with lower accumulation profiles such as isoniazid or streptomycin. These results indicate that the Myco-GEM model could serve as an intermediate platform to test new antibacterial chemotherapeutics for their ability to penetrate the complex cellular milieu of the granuloma.

The difficulty in directly targeting mycobacteria has led to a number of efforts to generate host-directed therapies for the treatment of mycobacterial disease[58]. These host-directed therapies have offered new approaches to treat mycobacterial disease and can enhance the activity and accessibility of existing therapies[23, 59–61]. In certain cases, these host-directed therapies can act by altering granuloma structure[62]. However, discovering these therapies is difficult and frequently requires the use of *in vivo* systems. Models including Myco-GEM that are faithful reporters of host response and are amenable to screening approaches could facilitate the discovery of new host-directed therapies.

Screening platforms that accurately model *in vivo* conditions are pivotal to the discovery of new therapies that are directly anti-mycobacterial. The substantial physiological reprogramming that occurs within mycobacteria during infection can render mycobacteria susceptible to therapies in the host that have no effect under standard *in vitro* growth conditions[63]. There is a growing recognition of the importance of developing models that reflect the *in vivo* cellular composition and reprogramming observed during mycobacterial infections[64]. Thus, the combination of chemical throughput, physiological context and the diversity of host and bacterial reporters available within the Myco-GEM model will enable screening for novel therapeutics.

Finally, in a targeted small molecule approach, we used the Myco-GEM platform to probe previous observations about the epithelialization of granuloma macrophages[4]. Using a validated chemical inhibitor of PKC signaling, we found that inhibition of this pathway in cultured granulomas led to rapid and dramatic loss of adherens junctions in granuloma macrophages, suggesting a role for PKC signaling in maintaining the epithelioid nature of granuloma macrophages.

More broadly, chemical genetic approaches can also be used to screen for pathways involved in many facets of granuloma function. To date, chemical screening approaches have been difficult and low-throughput in the context of an organized, mature granuloma *in vivo*. The large number of granulomas that can be tested in the Myco-GEM model will enable novel chemical-genetic approaches to study pathways involved in granuloma structure.

Mycobacterial granuloma structure and dynamics have been difficult to study directly, requiring challenging *in vivo* models and microscopy or *in vitro* surrogates that do not fully recapitulate *in vivo* granuloma features. Myco-GEM allows the culture of fully organized, mature granulomas, enabling longitudinal visualization of granuloma dynamics at resolutions and time frames that are unobtainable *in vivo* while retaining chemical and genetic access that is normally possible only *in vitro* or in cell culture. The Myco-GEM platform will facilitate new approaches to studying mycobacterial granuloma structure and dynamics and enable new screening approaches for bacterial and host-targeted therapies.

# Online Methods

## Zebrafish husbandry and strains

All zebrafish procedures were performed in accordance with the National Institutes of Health standards for the care and use of animals and were performed with the approval of the Duke University Animal Care and Use Committee (protocol A145–14-06). *Tg(ubb:loxp-tagbfp2-stop-loxp-tomato)*$^{xt7}$, *Tg(mfap4:icre-p2a-tomato)*$^{xt8}$, and *Gt(jupa-citrine)*$^{ct520a}$ zebrafish lines have all been previously described[4, 37]. *TgBAC(tnfa:gfp)*$^{pd1028}$ was a gift from Michel Bagnat (Duke University)[30]. *Tg(ubb:tomato)*$^{xt23}$ fish were made by Tol2 transgenesis. The *ubb:tomato* transgene was made by Gateway Multisite cloning[65], recombining p5E-*ubb*[66], pME-tomato[37], p3E-SV40 polyA[65] into pDEST-Tol2pA2[65]. Tol2 mRNA was transcribed using the mMessage mMachine T3 kit (Life Technologies) from pT3TS-Tol2[67].

## Adult zebrafish infection and *M. marinum* strains

Adult zebrafish were anesthetized by tricaine (MS-222, Syndel USA, final concentration 0.016% w/v). After anesthetization, zebrafish were injected intraperitoneally with 100–1000 fluorescent *M. marinum*/fish depending on strain and experiment in 10 μl or 15 μl of PBS with an insulin syringe. Both male and female zebrafish were used, aged between 2 and 24 months. Bacteria were prepared as single use frozen aliquots as previously described[68].

The *M. marinum* strains containing *msp12:tdtomato* and *msp12:wasabi* were a gift from Lalita Ramakrishnan (University of Cambridge). The *msp12:cerulean* M. marinum strain was previously published[23]. *M. marinum (hspX'::GFP, smyc'::mCherry)* was made by transforming *M. marinum* with the plasmid pCherry3-hspX::GFP[32], a gift from Robert Abramovitch.

## Granuloma culture and manipulation

A detailed protocol for Myco-GEM can be found in the Supplementary Protocol. Granulomas were collected from adult zebrafish between 2 and 4 weeks post infection depending on experiment. Collections at later time points generally gave larger numbers of granulomas that were of greater size. All manipulation of granulomas was done in plates that had been blocked with non-fat dry milk to minimize tissue adhesion to plasticware. After milk blocking, excess milk was removed by washing in distilled water, and plates were subsequently sterilized by treating with 70% ethanol, then washed two times in sterile 1× PBS.

Prior to euthanasia of animals and granuloma collection, a 96 well plate was freshly coated with Matrigel (Corning Life Sciences, 354262) by adding 40 μl of a 5 mg/ml solution of Matrigel to each well. Matrigel solutions were phenol red free, high concentration Matrigel diluted to 5 mg/ml in L-15 media and kept on ice. After Matrigel addition, the plate was left at room temperature for at least 20 minutes to enable Matrigel polymerization.

To collect granulomas, adult zebrafish were euthanized with a lethal dose of tricaine, surface sterilized by dipping the animal in 70% ethanol, washed once in PBS and both head and tail

were removed with a razor blade. The fish was placed in a milk blocked 100 mm plate filled with L-15 media. The body cavity was opened using forceps and granulomas were collected from the body cavity and internal organs using both microdissection from tissue by forceps and by pipetting tissue through a wide bore glass pipet. Granulomas were washed three times in L-15 media. Excess L-15 media was subsequently removed from the granulomas and the media was replaced with L-15 media containing 10% fetal bovine serum (Sigma, F2442) and 1 mg/ml Matrigel (top media) and transferred onto ice. Granulomas in top media were added to the wells of the Matrigel coated 96 well plate. Granulomas were positioned in the center of the well using a platinum wire. For granuloma consolidation experiments, granulomas were prepared as above and a single granuloma of each genotype was added to each well and the granulomas were positioned in contact with each other using a platinum wire.

Culture of granulomas on tissue culture plastic in Supplementary Figure 1a was done by plating granulomas in tissue culture treated 96 well plates in L-15 supplemented with 10% FBS.

Culture of granulomas embedded in agarose in Supplementary Figure 1b was done by suspending granulomas in 1% low melt agarose made in L-15 media containing 10% FBS and placed into wells of a 96 well plate. Granulomas were kept suspended in the 1% agarose solution until it solidified by using a platinum wire to manipulate the granulomas. Embedded granulomas were overlayed with L-15 containing 10% FBS.

For three-dimensional culture in Supplementary Figure 1c, granulomas were embedded in 5 mg/ml Matrigel by adding granulomas to a 5 mg/ml Matrigel solution at 4° C diluted with L-15, containing 10% FBS and subsequently added to wells of a 96 well plate. The granulomas were kept suspended through manipulation by a platinum wire until the Matrigel solidified. After solidification of the Matrigel, granulomas were overlayed with L-15 media containing 10% FBS.

For lightsheet microscopy, granulomas were transferred into 1.5% low melt agarose made in L-15 containing 0.01 mg/ml Matrigel. The granulomas were drawn into a capillary tube and agarose was allowed to set for at least 10 minutes prior to imaging.

For histology, granulomas were cultured for 6 days in 2.5D as described above. After the culture period, granulomas were excised from the Matrigel coated wells and fixed in 4% paraformaldehyde overnight. Granulomas were subsequently paraffin embedded, sectioned and stained with H&E by the Duke Research Immunohistology Lab. Histology of granulomas in whole fish was performed by fixing mycobacterial infected zebrafish in 4% paraformaldehyde for two days. Fixed fish were then paraffin embedded, sectioned and stained with H&E by the Duke Research Immunohistology Lab.

### Granuloma dissociation and analysis by flow cytometry

Granulomas were extracted from infected animals as described earlier. Granulomas were moved to a 1.5 mL tube and washed with PBS. Following PBS wash, granulomas were dissociated by adding 1 mL of 0.05% Trypsin/EDTA (ThermoFisher Scientific, 25300) and

incubating them at 30°C for 35–40 minutes with rocking. After dissociation, cells were washed 3 times by centrifuging for 5 min at 300×g followed by adding 1 ml PBS/5% fetal bovine serum (FBS). After washing, the cells were filtered through a 40 μm cell strainer. Cells were counted on a hemocytometer and cell suspensions were either immediately analyzed by flow cytometry directly (for granulomas from *tnfa:gfp* reporter animals) or subsequently stained with CellROX or LIVE/DEAD stain prior to analysis on a BD FACSCanto II. Flow plots were generated with FlowJo.

For CellROX staining, cells were stained for 30 min with 5 μM CellROX Green reagent (C10444, ThermoFisher Scientific). Cells were washed 3 times by centrifuging for 5 min at 300×g and subsequently adding 1 ml PBS. Cells were filtered through a 40 μm cell strainer and analyzed on a BD FACSCanto II. For LIVE/DEAD staining, cells were centrifuged at 300×g and washed in PBS twice, followed by staining with reconstituted LIVE/DEAD Near IR stain (L34975, ThermoFisher Scientific) for 30 min. After staining, cells were washed twice by centrifugation at 300×g followed by addition of 1 ml of PBS/5% FBS. After staining, cells were analyzed by flow cytometry on a BD FACSCanto II. The dead cell control sample was generated by incubating dissociated granuloma cells at 60°C for 10 min prior to staining with LIVE/DEAD stain.

### Cytospins of dissociated granuloma cells and staining

Cytospins were performed following standard procedures. Briefly, cell suspensions from dissociated granulomas were spun for 3 minutes at 800 rpm in a Shandon Cytospin3 apparatus. Slides were dried overnight at room temperature, and subsequently fixed in absolute methanol for 1 minute, stained with Wright-Giemsa (Sigma, WG16) for 1 minute, rinsed in ddH2O, then coverslipped with DPX mounting media (Sigma, 06522). Slides were imaged on a Zeiss AxioObserver Z.1 with an 40×/0.75 NA (Zeiss, EC Plan-Neofluar) and an ICc5 color camera (Zeiss) using Zen Blue 2012 edition (Zeiss).

### Construction of *(cdh1-tdtomato)$^{xt18}$* knockin zebrafish

E-cadherin knockin fish lines were made by the approach developed by Auer et al.[69]. zebrafish eggs at the 1 cell stage were injected with Cas9 mRNA and two gRNAs - one that targeted E-cadherin 3 amino acids upstream of the stop codon and a gRNA against GFP that targeted a coinjected plasmid, pUC19 GFPgRNA-Tomato-Ub polyA containing the tdTomato ORF. This plasmid results in the insertion of the entire pUC19 GFPgRNA-Tomato-Ub polyA starting at the GFP gRNA site directly upstream of the Tomato ORF. For injections, ~1 nl of an injection mix consisting of 50 ng/μl of each of the gRNAs, pUC19 GFPgRNA-Tomato-Ub at 12 ng/μl and Cas9 mRNA at 150 ng/μl was injected into each single cell embryo. Injected animals were screened at 2 dpf for fluorescence positive animals and animals were raised to adulthood. Injected animals were subsequently outcrossed to identify founder animals and the insertion alleles were sequenced. An insertion allele was identified in which the two penultimate residues, a glycine and a glutamate, were deleted during NHEJ insertion, but the final amino acid, an aspartate, was rescued with sequence from the insertion construct. These changes resulted in changing the c-terminus of E-cadherin from GGGED to GGD which is directly fused to the sequence of tdTomato.

The gRNA targeting the site 5′-GGACATGTATGGAGGAGGAGAGG-3′ (Underlined characters denote the PAM sequence) in E-cadherin was made by annealing the oligo 5′-taatacgactcactataGGACATGTATGGAGGAGGAGgttttagagctagaa-3′ with an oligo containing the gRNA 3' constant region by the method of Moreno-Mateos[70]. The gRNA targeting the site 5′-GGCGAGGGCGATGCCACCTACGG-3′ in GFP was made by annealing the oligo 5′-taatacgactcactataGGCGAGGGCGATGCCACCTAgttttagagctagaa-3′ with the oligo encoding the gRNA constant region as was done for E-cadherin. gRNAs were synthesized by *in vitro* transcription using the MEGAshortscript T7 kit (ThermoFisher Scientific, AM1354).

## CLARITY tissue clearing and staining of dissected granulomas

Granulomas were dissected and fixed in a modified CLARITY solution (1% Acrylamide, 0.5% bis-Acrylamide, 4% paraformaldehyde, 0.25% VA-044 in 1× PBS). Following overnight incubation in CLARITY solution at 4°C, CLARITY hydrogel solution was polymerized for 3 hours at 37 °C. Granulomas were retrieved from CLARITY solution and washed 3 times in 1× PBS. CLARITY embedded granulomas were subsequently incubated overnight at 37 °C in 8% SDS/200 mM Boric acid with shaking. After overnight SDS incubation, the granulomas were washed twice in PBS/0.1% Triton X-100 (PBS-T) overnight and subsequently equilibrated overnight in refractive index matching solution (RIMS, 88% Histodenz (Sigma, D2158), 0.02M Phosphate buffer, pH 7.5, 0.01% Sodium Azide, 2.7 μg/ml Hoechst 33258). For neutrophil staining, after PBS-T washes, granulomas were stained overnight in 1:100 rabbit anti-LysC (Anaspec, AS-55633). Stained granulomas were washed overnight with PBS-T, stained overnight with 1:100 Alexa 647 labeled goat anti-rabbit antibody (ThermoFisher, A21245) and washed overnight in PBS-T. Stained granulomas were equilibrated overnight in RIMS as previously described.

## Imaging

Epifluorescent imaging of granulomas was conducted on an inverted Zeiss AxioObserverZ.1 using a 20× long working distance/0.4 NA lens (Zeiss, LD Plan NeoFluar), a Zeiss MRm camera and either an Xcite 120Q or an Xcite 120LED (Lumen Dynamics) light source. Images were acquired using the Zen Blue 2012 imaging suite (Zeiss).

Confocal images were acquired on an Andor XD spinning disk confocal, consisting of an Olympus IX81 inverted microscope equipped with a Yokogawa CSU-X1 spinning disk using a 20×/0.5 UplanFl lens (Olympus) and detected with a Andor Ixon3 897 EMCCD. Images were acquired using Metamorph.

Confocal images of CLARITY cleared granulomas and granulomas from (cdh1-tdtomato)$^{xt18}$ animals were obtained on a Zeiss AxioObserverZ.1 equipped with an XLIGHT V2 spinning disk unit (Crest Optics, Rome, Italy) using a 20×/0.5 NA lens, an ORCA Flash4.0 V3 (Hamamatsu, Bridgewater, NJ) and an LDI multiline laser (89 North, Williston VT).

Lightsheet microscopy was performed on a Zeiss Lightsheet Z1 using a Plan-Apochromat 20×/1.0 NA Aqueous immersion objective and a PCO.edge camera. Individual channels were acquired sequentially using dual-side illumination.

For presentation, images were prepared and adjusted using Zen software and FIJI for contrast adjustments and maximum projections.

## Isotopic labeling of lipids in granulomas

To coat wells, high concentration Matrigel solutions were diluted to 5 mg/ml in DMEM containing either 4.5 g/L $^{13}C$ or $^{12}C$ glucose. Granulomas were dissected from adult zebrafish and washed as outlined above. After three washes in L-15 media, the media on the granulomas was exchanged to DMEM supplemented with 4.5 g/L $^{13}C$ glucose, 10% fetal bovine serum and 1 mg/ml Matrigel. Control granulomas were treated identically except supplemented with 4.5 g/L $^{12}C$ glucose in place of $^{13}C$ glucose. Granulomas were plated in individual wells of a 96 well plate coated with 5 mg/ml Matrigel as outlined above and cultured for 2 or 4 days in a humidified incubator at 30°C/5% $CO_2$. After 2 or 4 days of culture, individual granulomas were excised from the Matrigel substrate with a platinum wire and snap frozen in the vapor phase of liquid nitrogen. Granulomas were stored at −80°C until analysis.

For granulomas that were shifted from $^{12}C$ glucose to$^{13}C$ glucose after 4 days, granulomas were cultured as above in DMEM with 4.5 g/L $^{12}C$ glucose, 10% fetal bovine serum and 1 mg/ml Matrigel. At day 4, media was carefully removed with a pipet and replaced with 250 μl of DMEM supplemented with 4.5 g/L $^{13}C$ glucose, 10% fetal bovine serum and 1 mg/ml Matrigel. Fresh DMEM supplemented with 4.5 g/L $^{12}C$ glucose, 10% fetal bovine serum and 1 mg/ml Matrigel was added to control granulomas.

## MALDI mass spectrometry data acquisition

Snap frozen granuloma were thaw-mounted onto stainless steel slides. Di-aminonapthalene (DAN) MALDI matrix was applied to the tissues using a TM-Sprayer automated MALDI tissue prep device (HTX Technologies, NC) under the following optimized conditions: DAN 5 mg/ml in Acetone/water 7:3, 0.05-mL/min flow rate, 60°C nozzle temperature, and 1.3-mm/s raster speed, with 20 passes over the granuloma.

MALDI acquisition was performed using a MALDI LTQ Orbitrap XL mass spectrometer (Thermo Fisher Scientific, Bremen, Germany) with a resolution of 60,000 at m/z 400, full width at half maximum. MS Spectra were acquired in negative mode across the mass range m/z 500–2500 with a laser energy of 10 μJ and 5 shots per position (1 microscan per position). MS/MS analysis was performed on peaks present at m/z 885.55 (putatively identified as PI-38:4 based on the Human Metabolome Data Base within a ±0.001 Da mass tolerance window) and m/z 888.56. To confirm the identity of these peaks, a precursor isolation window of 1 m/z was selected and a collision energy of 30 was selected for collision induced dissociation. Dissociation produced ions were acquired between m/z 240 and m/z 900.

### Bioluminescence Assay

A bioluminescent reporter strain of *Mm* (*Mm*-Lux) was created by introducing the plasmid construct pMV306hsp+LuxG13 containing the bacterial luciferase operon plus the *Mm* G13 promoter[40] which was a gift from Brian Robertson and Siouxsie Wiles (Addgene plasmid #26161, Cambridge, MA) of the *M. marinum* M strain. Granulomas from *Mm*-Lux infected adult zebrafish were cultured in white-walled, polystyrene, clear bottom, 96 well, half area cell culture microplates (Greiner Bio-one, 655075) and luminescence was measured with an EnSpire 2300 Multilabel Plate Reader (Perkin Elmer, Waltham, MA). Values were expressed in relative light units (RLU).

For anti-mycobacterial therapy studies, the indicated concentrations of anti-mycobacterials were added to top media and drug-containing top media was subsequently added to granulomas. All tuberculosis chemotherapeutics were dissolved in L-15 media with the exception of rifampcin, rifapentine and bedaquiline which were dissolved in DMSO. Control granulomas were treated with an equivalent amount of vehicle. For experiments in which drugs were dissolved in DMSO, all conditions were normalized to 0.1% DMSO.

### Granuloma colony forming unit assay

Individual granulomas were isolated from culture and placed into microcentrifuge tubes containing two sterile glass beads in 100 µl of 7H9 media then homogenized by vortexing. Homogenates were plated on 7H10 media (BD Difco, Franklin Lakes, NJ) containing 20 µg/ml kanamycin and incubated at 30°C for 14 days before enumeration of bacterial colonies.

### *Ex vivo* granuloma transfection

Granulomas were collected and washed as outlined in Granuloma Culture and Manipulation. Prior to transfer to top media, the granulomas were placed in PCR tubes in ~80 µl L-15/10% fetal bovine serum. The granulomas were subsequently transfected with 200 ng of tdTomato mRNA using ViromerRED (Lipocalyx, VR-01LB-01) according to suspension cell conditions. RNA for transfections was transcribed using the mMessage mMachine T3 kit (Life Technologies) from T3TS-tdTomato. Transcribed RNA was subsequently polyadenylated with *E. coli* poly(A) polymerase (NEB, M0276) and frozen in single use aliquots at −80° C. pT3TS-tdTomato was made by amplifying the tdTomato open reading frame from pME-tomato[37] and the T3TS plasmid backbone from pT3TS-Tol2[67] to clone tdTomato in place of Tol2 using In-Fusion cloning (Takara). Primers used were `5′-TTTGGCAGATCCACCATGGTGAGCAAGGGCGAGGA-3′` and `5′-TAGTCAGTCACTAGTTTACTTGTACAGCTCGTCCATG-3′` to amplify tomato and `5′-GAGCTGTACAAGTAAACTAGTGACTGACTAGGATCTG-3′` and `5′-GCCCTTGCTCACCATGGTGGATCTGCCAAAGTTGAG-3′` to amplify the T3TS backbone.

### Gö6983 treatment of granulomas

Gö6983 was purchased from LC labs (cat no G-7700) and stocks were made in DMSO at 10 mM. For lightsheet analysis of Gö6983 treated granulomas, freshly dissected granulomas were embedded in 1.5% low melt agarose made in L-15 with 0.01 mg/ml Matrigel

containing 10 μM Gö6983 or, for control granulomas, DMSO vehicle alone. During lightsheet imaging, the imaging chamber surrounding the agarose plug was filled with L-15 containing 10 μM Gö6983 or an equivalent amount of DMSO vehicle for controls.

### Statistics

Statistical analysis was done by one-way ANOVA with Tukey's multiple comparison test using Prism 7 (GraphPad Software). Significance and sample sizes are indicated in figure legends. A p-value of less than 0.05 was the threshold for statistical significance.

## Supplementary Material

Refer to Web version on PubMed Central for supplementary material.

## Acknowledgements

We are grateful to members of the Tobin laboratory and J. Stout for helpful discussions, E. Hughes for critical reading of the granuloma protocol, E. Hunt for fish care, A. Piro and J. Coers for reagents, R. Abramovitch for the HspX reporter plasmid, and D. Russell for suggesting RNA transfection of granuloma macrophages. This work was supported by an American Cancer Society Postdoctoral Fellowship PF-13–223-01-MPC (M.R.C.); an NSF Graduate Research Fellowship (M.A.M.); NIH NRSA 1F32AI124658–01A1 (A.F.R) and NIH grants AI130236, AI125517, AI127115 (D.M.T.) and 5P01DK094779–05 (J.F.R.), and a Vallee Scholar Award (D.M.T.).

## References

1. Ramakrishnan L Revisiting the role of the granuloma in tuberculosis. Nat Rev Immunol 12, 352–366 (2012). [PubMed: 22517424]
2. Lenaerts A, Barry CE, 3rd & Dartois V Heterogeneity in tuberculosis pathology, microenvironments and therapeutic responses. Immunol Rev 264, 288–307 (2015). [PubMed: 25703567]
3. Adams DO The structure of mononuclear phagocytes differentiating in vivo. I. Sequential fine and histologic studies of the effect of Bacillus Calmette-Guerin (BCG). Am J Pathol 76, 17–48 (1974). [PubMed: 4601921]
4. Cronan MR et al. Macrophage Epithelial Reprogramming Underlies Mycobacterial Granuloma Formation and Promotes Infection. Immunity 45, 861–876 (2016). [PubMed: 27760340]
5. Mattila JT et al. Microenvironments in tuberculous granulomas are delineated by distinct populations of macrophage subsets and expression of nitric oxide synthase and arginase isoforms. J Immunol 191, 773–784 (2013). [PubMed: 23749634]
6. Wolf AJ et al. Mycobacterium tuberculosis infects dendritic cells with high frequency and impairs their function in vivo. J Immunol 179, 2509–2519 (2007). [PubMed: 17675513]
7. Volkman HE et al. Tuberculous granuloma formation is enhanced by a mycobacterium virulence determinant. PLoS Biol 2, e367 (2004). [PubMed: 15510227]
8. Davis JM & Ramakrishnan L The role of the granuloma in expansion and dissemination of early tuberculous infection. Cell 136, 37–49 (2009). [PubMed: 19135887]
9. Lin PL et al. Sterilization of granulomas is common in active and latent tuberculosis despite within-host variability in bacterial killing. Nat Med 20, 75–79 (2014). [PubMed: 24336248]
10. Samstein M et al. Essential yet limited role for CCR2(+) inflammatory monocytes during Mycobacterium tuberculosis-specific T cell priming. Elife 2, e01086 (2013). [PubMed: 24220507]
11. Wolf AJ et al. Initiation of the adaptive immune response to Mycobacterium tuberculosis depends on antigen production in the local lymph node, not the lungs. J Exp Med 205, 105–115 (2008). [PubMed: 18158321]
12. Harding JS, Rayasam A, Schreiber HA, Fabry Z & Sandor M Mycobacterium-Infected Dendritic Cells Disseminate Granulomatous Inflammation. Sci Rep 5, 15248 (2015). [PubMed: 26515292]

13. Malherbe ST et al. Persisting positron emission tomography lesion activity and Mycobacterium tuberculosis mRNA after tuberculosis cure. Nat Med 22, 1094–1100 (2016). [PubMed: 27595324]
14. Coleman MT et al. PET/CT imaging reveals a therapeutic response to oxazolidinones in macaques and humans with tuberculosis. Sci Transl Med 6, 265ra167 (2014).
15. Egen JG et al. Intravital imaging reveals limited antigen presentation and T cell effector function in mycobacterial granulomas. Immunity 34, 807–819 (2011). [PubMed: 21596592]
16. Torabi-Parizi P et al. Pathogen-related differences in the abundance of presented antigen are reflected in CD4+ T cell dynamic behavior and effector function in the lung. J Immunol 192, 1651–1660 (2014). [PubMed: 24431231]
17. Egen JG et al. Macrophage and T cell dynamics during the development and disintegration of mycobacterial granulomas. Immunity 28, 271–284 (2008). [PubMed: 18261937]
18. Guirado E et al. Characterization of host and microbial determinants in individuals with latent tuberculosis infection using a human granuloma model. MBio 6, e02537–02514 (2015). [PubMed: 25691598]
19. Puissegur MP et al. An in vitro dual model of mycobacterial granulomas to investigate the molecular interactions between mycobacteria and human host cells. Cell Microbiol 6, 423–433 (2004). [PubMed: 15056213]
20. Tezera LB et al. Dissection of the host-pathogen interaction in human tuberculosis using a bioengineered 3-dimensional model. Elife 6 (2017).
21. Birkness KA et al. An in vitro model of the leukocyte interactions associated with granuloma formation in Mycobacterium tuberculosis infection. Immunol Cell Biol 85, 160–168 (2007). [PubMed: 17199112]
22. Davis JM et al. Real-time visualization of mycobacterium-macrophage interactions leading to initiation of granuloma formation in zebrafish embryos. Immunity 17, 693–702 (2002). [PubMed: 12479816]
23. Oehlers SH et al. Interception of host angiogenic signalling limits mycobacterial growth. Nature 517, 612–615 (2015). [PubMed: 25470057]
24. Swaim LE et al. Mycobacterium marinum infection of adult zebrafish causes caseating granulomatous tuberculosis and is moderated by adaptive immunity. Infect Immun 74, 6108–6117 (2006). [PubMed: 17057088]
25. Parikka M et al. Mycobacterium marinum causes a latent infection that can be reactivated by gamma irradiation in adult zebrafish. PLoS Pathog 8, e1002944 (2012). [PubMed: 23028333]
26. Cronan MR et al. CLARITY and PACT-based imaging of adult zebrafish and mouse for whole-animal analysis of infections. Dis Model Mech 8, 1643–1650 (2015). [PubMed: 26449262]
27. Flynn JL et al. Tumor necrosis factor-alpha is required in the protective immune response against Mycobacterium tuberculosis in mice. Immunity 2, 561–572 (1995). [PubMed: 7540941]
28. Lin PL et al. Tumor necrosis factor neutralization results in disseminated disease in acute and latent Mycobacterium tuberculosis infection with normal granuloma structure in a cynomolgus macaque model. Arthritis Rheum 62, 340–350 (2010). [PubMed: 20112395]
29. Clay H, Volkman HE & Ramakrishnan L Tumor necrosis factor signaling mediates resistance to mycobacteria by inhibiting bacterial growth and macrophage death. Immunity 29, 283–294 (2008). [PubMed: 18691913]
30. Marjoram L et al. Epigenetic control of intestinal barrier function and inflammation in zebrafish. Proc Natl Acad Sci U S A 112, 2770–2775 (2015). [PubMed: 25730872]
31. Shapouri-Moghaddam A et al. Macrophage plasticity, polarization, and function in health and disease. J Cell Physiol 233, 6425–6440 (2018).
32. Tan S, Sukumar N, Abramovitch RB, Parish T & Russell DG Mycobacterium tuberculosis responds to chloride and pH as synergistic cues to the immune status of its host cell. PLoS Pathog 9, e1003282 (2013). [PubMed: 23592993]
33. Tan S & Russell DG Trans-species communication in the Mycobacterium tuberculosis-infected macrophage. Immunol Rev 264, 233–248 (2015). [PubMed: 25703563]
34. Philips JA & Ernst JD Tuberculosis pathogenesis and immunity. Annu Rev Pathol 7, 353–384 (2012). [PubMed: 22054143]

35. Marakalala MJ et al. Inflammatory signaling in human tuberculosis granulomas is spatially organized. Nat Med 22, 531–538 (2016). [PubMed: 27043495]
36. Zhurinsky J, Shtutman M & Ben-Ze'ev A Plakoglobin and beta-catenin: protein interactions, regulation and biological roles. J Cell Sci 113 **(** Pt 18**)**, 3127–3139 (2000). [PubMed: 10954412] **()**
37. Walton EM, Cronan MR, Beerman RW & Tobin DM The Macrophage-Specific Promoter mfap4 Allows Live, Long-Term Analysis of Macrophage Behavior during Mycobacterial Infection in Zebrafish. PLoS One 10, e0138949 (2015). [PubMed: 26445458]
38. Martin CJ et al. Digitally Barcoding Mycobacterium tuberculosis Reveals In Vivo Infection Dynamics in the Macaque Model of Tuberculosis. MBio 8 (2017).
39. Dartois V The path of anti-tuberculosis drugs: from blood to lesions to mycobacterial cells. Nat Rev Microbiol 12, 159–167 (2014). [PubMed: 24487820]
40. Andreu N et al. Optimisation of bioluminescent reporters for use with mycobacteria. PLoS One 5, e10777 (2010). [PubMed: 20520722]
41. Cosma CL, Klein K, Kim R, Beery D & Ramakrishnan L Mycobacterium marinum Erp is a virulence determinant required for cell wall integrity and intracellular survival. Infect Immun 74, 3125–3133 (2006). [PubMed: 16714540]
42. Adams KN et al. Drug tolerance in replicating mycobacteria mediated by a macrophage-induced efflux mechanism. Cell 145, 39–53 (2011). [PubMed: 21376383]
43. Rodriguez-Boulan E & Macara IG Organization and execution of the epithelial polarity programme. Nat Rev Mol Cell Biol 15, 225–242 (2014). [PubMed: 24651541]
44. Sato K et al. Numb controls E-cadherin endocytosis through p120 catenin with aPKC. Mol Biol Cell 22, 3103–3119 (2011). [PubMed: 21775625]
45. Winograd-Katz SE, Fassler R, Geiger B & Legate KR The integrin adhesome: from genes and proteins to human disease. Nat Rev Mol Cell Biol 15, 273–288 (2014). [PubMed: 24651544]
46. Tobin DM et al. The lta4h locus modulates susceptibility to mycobacterial infection in zebrafish and humans. Cell 140, 717–730 (2010). [PubMed: 20211140]
47. Bafica A et al. Host control of Mycobacterium tuberculosis is regulated by 5-lipoxygenase-dependent lipoxin production. J Clin Invest 115, 1601–1606 (2005). [PubMed: 15931391]
48. Chen M et al. Lipid mediators in innate immunity against tuberculosis: opposing roles of PGE2 and LXA4 in the induction of macrophage death. J Exp Med 205, 2791–2801 (2008). [PubMed: 18955568]
49. Mayer-Barber KD et al. Host-directed therapy of tuberculosis based on interleukin-1 and type I interferon crosstalk. Nature 511, 99–103 (2014). [PubMed: 24990750]
50. Subbian S et al. Chronic pulmonary cavitary tuberculosis in rabbits: a failed host immune response. Open Biol 1, 110016 (2011). [PubMed: 22645653]
51. Ellett F, Pase L, Hayman JW, Andrianopoulos A & Lieschke GJ mpeg1 promoter transgenes direct macrophage-lineage expression in zebrafish. Blood 117, e49–56 (2011). [PubMed: 21084707]
52. Prideaux B et al. The association between sterilizing activity and drug distribution into tuberculosis lesions. Nat Med 21, 1223–1227 (2015). [PubMed: 26343800]
53. Zimmerman M et al. Ethambutol Partitioning in Tuberculous Pulmonary Lesions Explains Its Clinical Efficacy. Antimicrob Agents Chemother 61 (2017).
54. Irwin SM et al. Bedaquiline and Pyrazinamide Treatment Responses Are Affected by Pulmonary Lesion Heterogeneity in Mycobacterium tuberculosis Infected C3HeB/FeJ Mice. ACS Infect Dis 2, 251–267 (2016). [PubMed: 27227164]
55. Mor N, Simon B, Mezo N & Heifets L Comparison of activities of rifapentine and rifampin against Mycobacterium tuberculosis residing in human macrophages. Antimicrob Agents Chemother 39, 2073–2077 (1995). [PubMed: 8540718]
56. Bonventre PF, Hayes R & Imhoff J Autoradiographic evidence for the impermeability of mouse peritoneal macrophages to tritiated streptomycin. J Bacteriol 93, 445–450 (1967). [PubMed: 6020415]
57. Tulkens PM Intracellular distribution and activity of antibiotics. Eur J Clin Microbiol Infect Dis 10, 100–106 (1991). [PubMed: 1864271]

58. Hawn TR, Matheson AI, Maley SN & Vandal O Host-directed therapeutics for tuberculosis: can we harness the host? Microbiol Mol Biol Rev 77, 608–627 (2013). [PubMed: 24296574]

59. Datta M et al. Anti-vascular endothelial growth factor treatment normalizes tuberculosis granuloma vasculature and improves small molecule delivery. Proc Natl Acad Sci U S A 112, 1827–1832 (2015). [PubMed: 25624495]

60. Napier RJ et al. Imatinib-sensitive tyrosine kinases regulate mycobacterial pathogenesis and represent therapeutic targets against tuberculosis. Cell Host Microbe 10, 475–485 (2011). [PubMed: 22100163]

61. Xu Y et al. Matrix metalloproteinase inhibitors enhance the efficacy of frontline drugs against Mycobacterium tuberculosis. PLoS pathogens 14, e1006974 (2018). [PubMed: 29698476]

62. Gautam US et al. In vivo inhibition of tryptophan catabolism reorganizes the tuberculoma and augments immune-mediated control of Mycobacterium tuberculosis. Proc Natl Acad Sci U S A 115, E62–E71 (2018). [PubMed: 29255022]

63. VanderVen BC et al. Novel inhibitors of cholesterol degradation in Mycobacterium tuberculosis reveal how the bacterium's metabolism is constrained by the intracellular environment. PLoS Pathog 11, e1004679 (2015). [PubMed: 25675247]

64. Huang L et al. The Deconstructed Granuloma: A Complex High-Throughput Drug Screening Platform for the Discovery of Host-Directed Therapeutics Against Tuberculosis. Frontiers in Cellular and Infection Microbiology 8 (2018).

## Methods-only References

65. Kwan KM et al. The Tol2kit: a multisite gateway-based construction kit for Tol2 transposon transgenesis constructs. Dev Dyn 236, 3088–3099 (2007). [PubMed: 17937395]

66. Mosimann C et al. Ubiquitous transgene expression and Cre-based recombination driven by the ubiquitin promoter in zebrafish. Development 138, 169–177 (2011). [PubMed: 21138979]

67. Balciunas D et al. Harnessing a high cargo-capacity transposon for genetic applications in vertebrates. PLoS Genet 2, e169 (2006). [PubMed: 17096595]

68. Takaki K, Davis JM, Winglee K & Ramakrishnan L Evaluation of the pathogenesis and treatment of Mycobacterium marinum infection in zebrafish. Nat Protoc 8, 1114–1124 (2013). [PubMed: 23680983]

69. Auer TO, Duroure K, De Cian A, Concordet JP & Del Bene F Highly efficient CRISPR/Cas9-mediated knock-in in zebrafish by homology-independent DNA repair. Genome Res 24, 142–153 (2014). [PubMed: 24179142]

70. Moreno-Mateos MA et al. CRISPRscan: designing highly efficient sgRNAs for CRISPR-Cas9 targeting in vivo. Nat Methods 12, 982–988 (2015). [PubMed: 26322839]

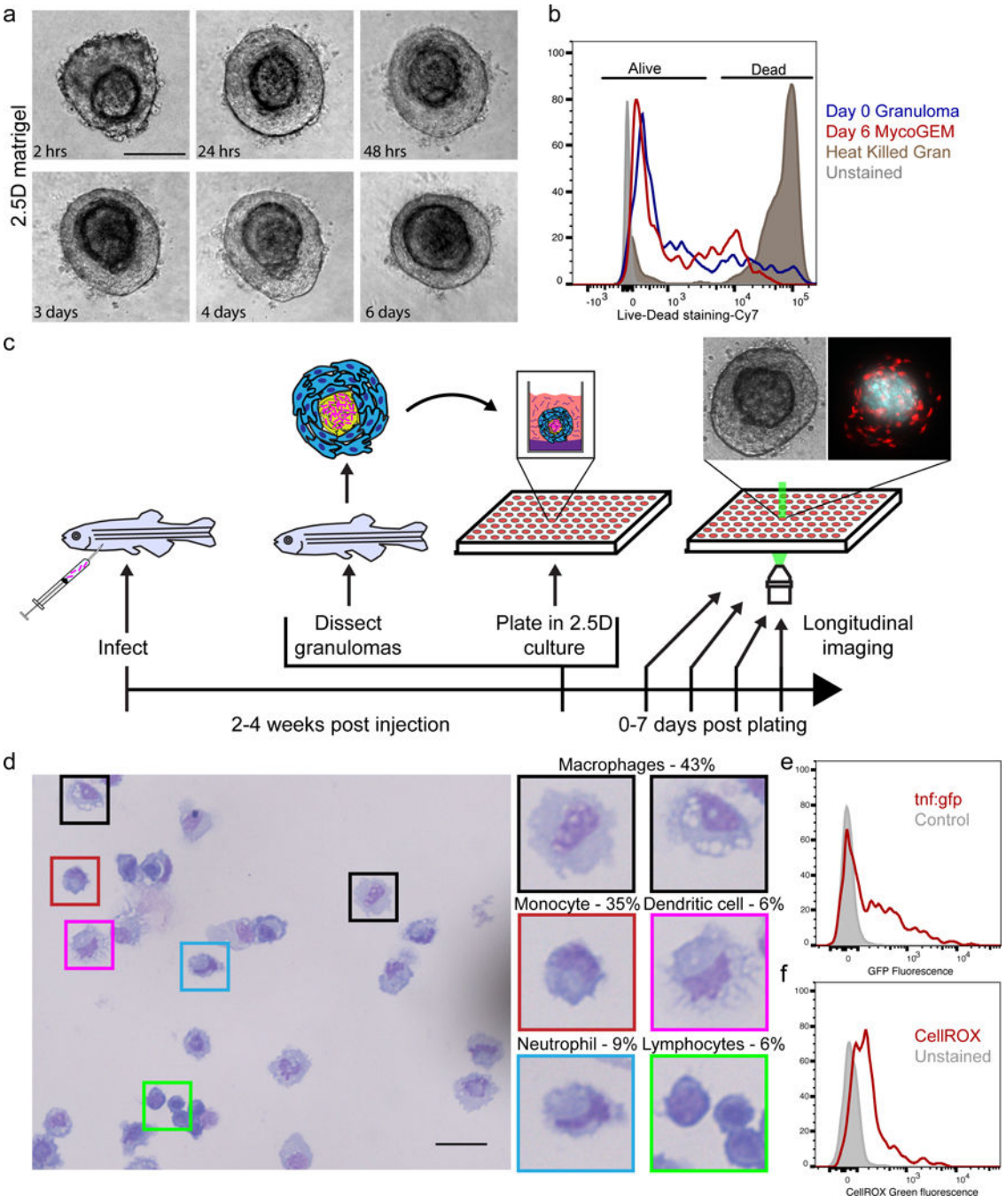


**Figure 1.**

Ex vivo granuloma cultured granulomas retain *in vivo* organization and can be longitudinally imaged. (a) Phase contrast images of a single granuloma from 2 hours post plating to 6 days post plating as indicated. Images are representative of 4 independent experiments with similar results. Scale bar – 100 μm. (b) Flow cytometry analysis of LIVE/DEAD staining of freshly dissected granulomas (blue) and granulomas cultured for 6 days in Myco-GEM (red). Heat killed, disaggregated granuloma cells are shown as a positive control for LIVE/DEAD staining (brown) while unstained, disaggregated granuloma cells (grey) are

shown as a negative control. Similar flow cytometry results were seen in 3 independent experiments. (c) Schematic illustrating the overall workflow of the Myco-GEM model. (d) Granulomas were disaggregated and cytospun preparations were stained with Wright-Giemsa. Left – a representative image of a field of stained, cytospun granuloma cells. Colored boxes indicate cell types depicted in magnified images on the right. Right – representative images of cell types identified in cytospins. Percentages are the mean percentage of each cell type from counts of cytospins from two different, independent pools of granulomas. Each pool of granulomas was derived from at least 20 granulomas from a separate animal. A minimum of 200 cells were counted for each pool of granulomas. Scale bar – 25 μm. (e,f) Flow cytometry analysis of inflammatory markers in dissociated granuloma populations. Similar results were obtained from 3 independent experiments. (e) Analysis of TNF GFP reporter expression in disaggregated granulomas from *tnfa:gfp* animals (red) or disaggregated granulomas from wildtype *AB control animals (grey). (f) Analysis of reactive oxygen species within the cells comprising the granuloma. Disaggregated cells from granulomas formed in wildtype animals were either stained with CellROX (red) or unstained as a negative control (grey).

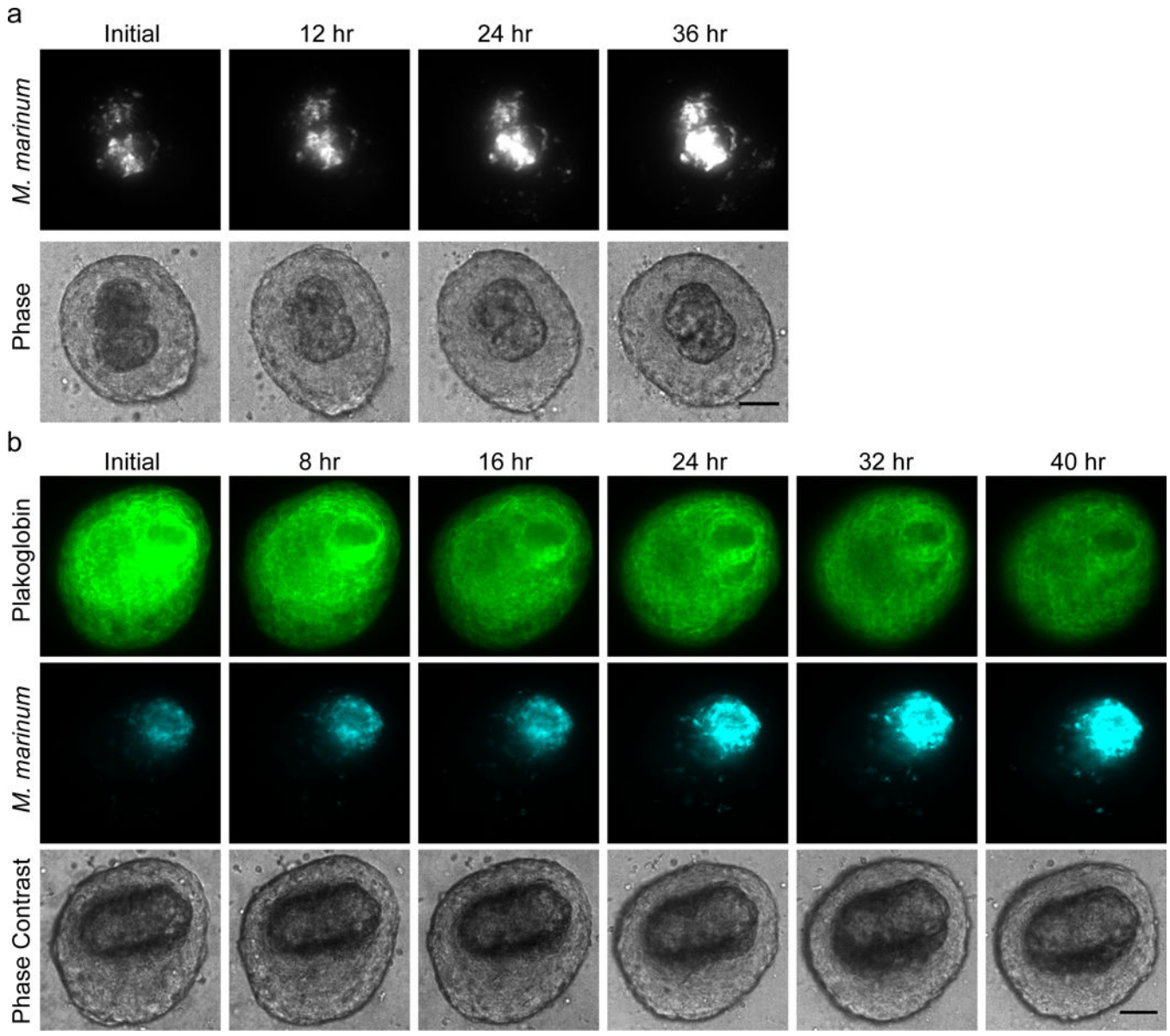


**Figure 2.**

Bacterial replication and granuloma epithelialization are retained under Myco-GEM culture conditions. (a) Images of a cultured granuloma showing phase contrast and fluorescent *M. marinum*. Phase contrast images are each from a single z-plane, while fluorescent *M. marinum* images are maximum projections of a 70 μm z-stack of the volume of the granuloma. Similar results were observed in 5 independent experiments. Scale bar – 50 μm. (b) Single z-plane images of granulomas from plakoglobin-citrine animals showing adherens junctions (green) *M. marinum* (cyan) and phase contrast images. Granulomas were imaged from 0 to 40 hours post plating as indicated. Results were representative of 4 independent experiments. Scale bar – 50 μm.

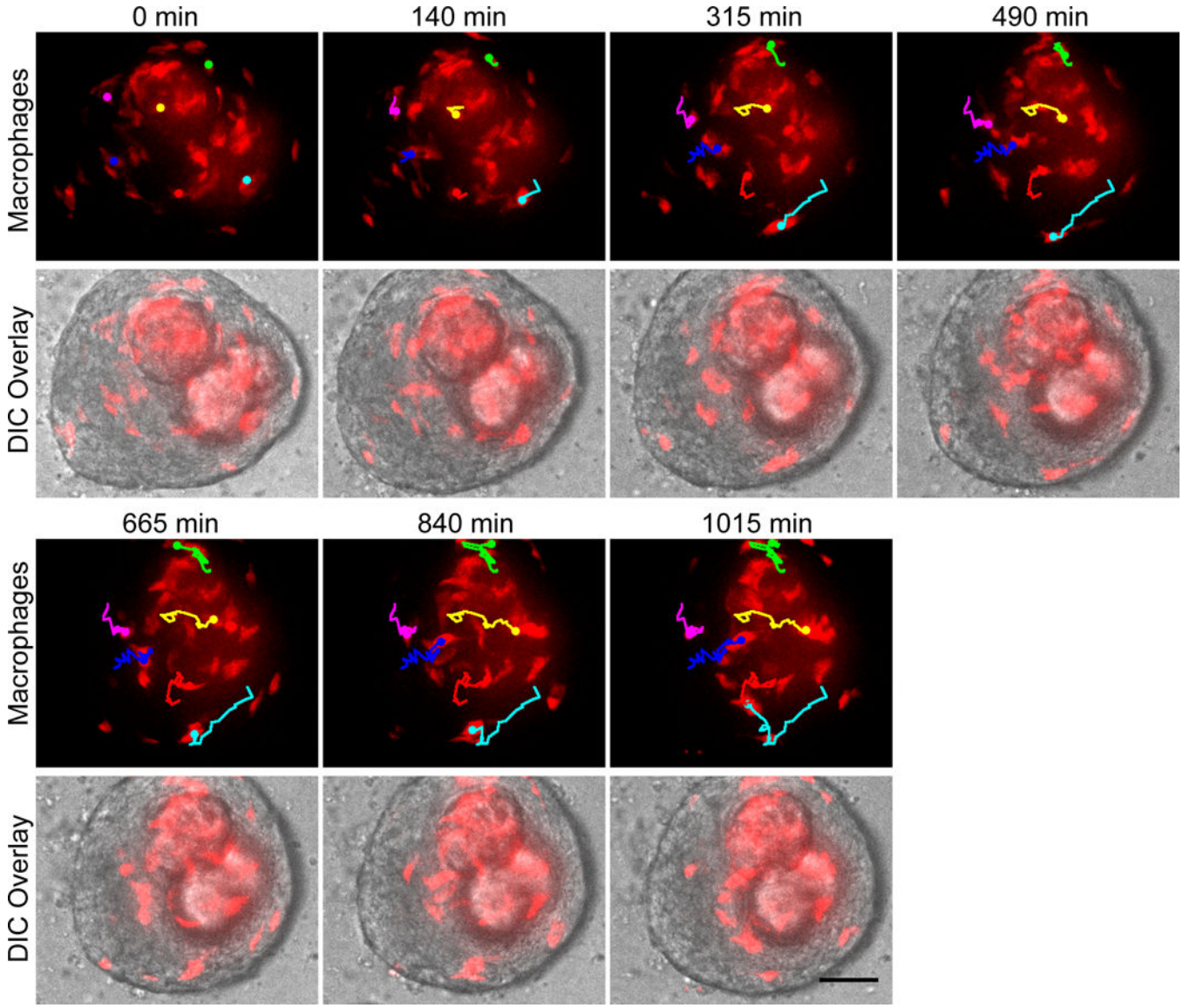


**Figure 3.**

Macrophage dynamics within cultured granulomas. Macrophages (red) marked by macrophage lineage tracing were tracked within the granuloma over the course of 17 hours. Individual dots and colored lines indicate the frame-to-frame position of an individual macrophage. Macrophage images are a maximum projection of a 68 μm z-stack. DIC images are single plane images from the center of the granuloma. Similar microscopy results were observed in 3 independent experiments. Scale bar – 50 μm.

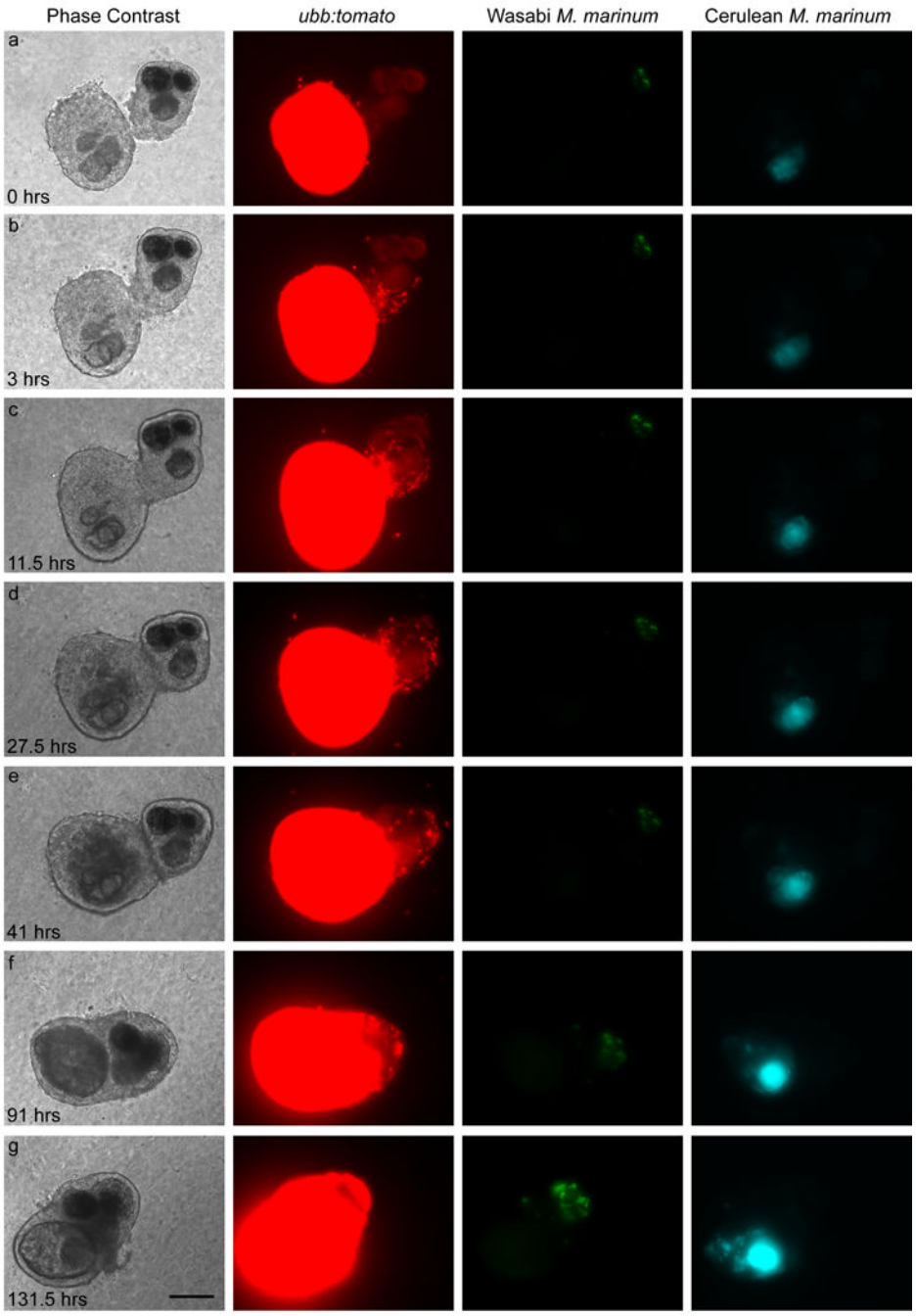


**Figure 4.**

Granulomas undergo consolidation during *ex vivo* culture. A granuloma that ubiquitously expresses tomato fluorescent protein within its constituent cells (*Tg(ubb:tomato)*, red) and from an animal infected with cerulean-expressing *M. marinum* (cyan) was placed in contact with an unlabeled granuloma containing wasabi expressing *M. marinum* (green). Granulomas were imaged during granuloma consolidation over 6 days of co-culture. Phase images are from single planes near the center of the granuloma, Tomato and *M. marinum*

images are maximum projections of 70 μm z-stacks. Granuloma consolidation was repeated 4 independent times with similar results. Scale bar – 100 μm.

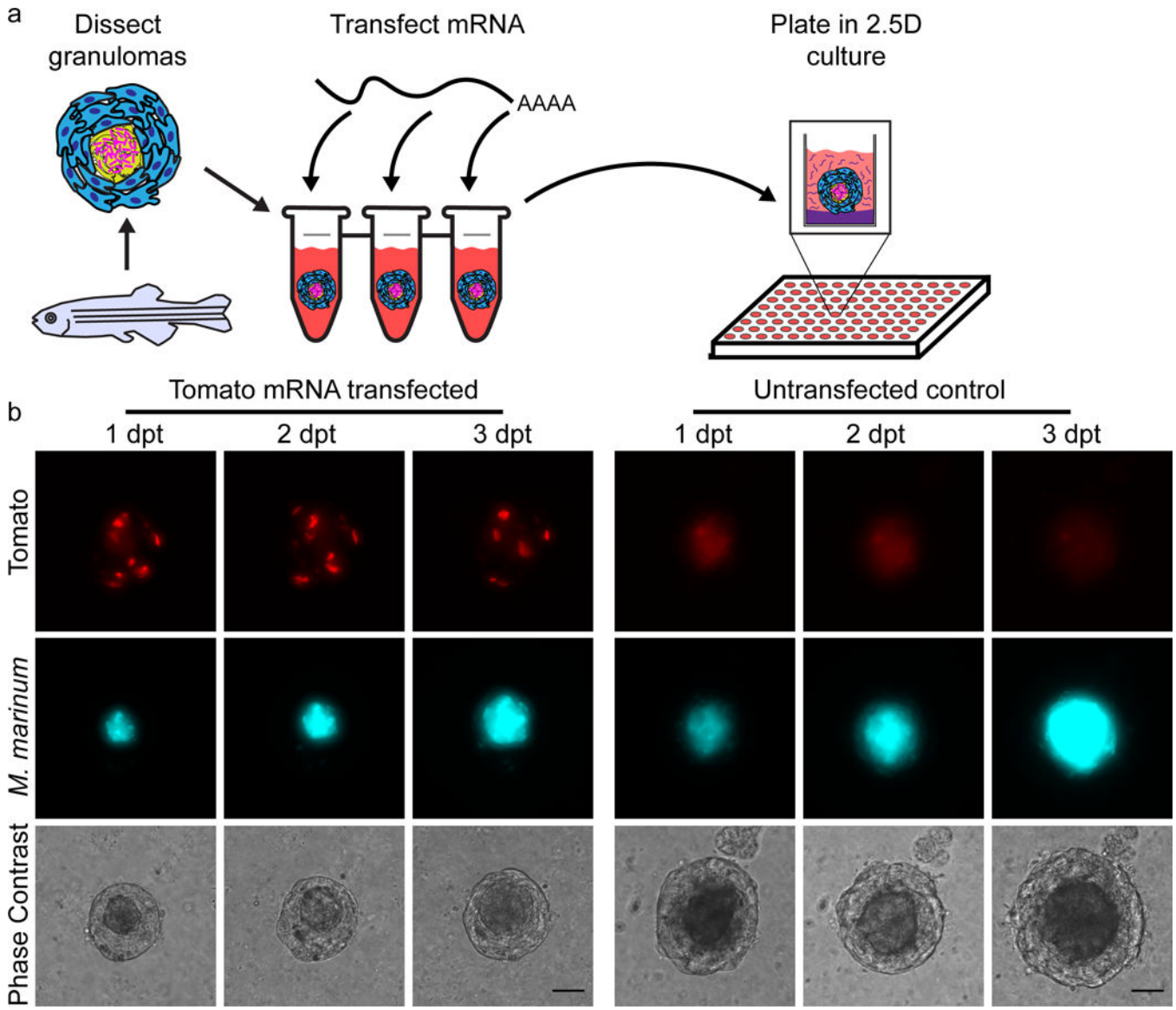


**Figure 5.**

Granuloma transfection allows genetic manipulation of *ex vivo* cultured granulomas. (a) Schematic illustrating the transfection protocol used for transfecting granulomas. (b) Untransfected and tdTomato mRNA-transfected (red) granulomas containing fluorescent *M. marinum* (cyan). Individual granulomas were followed from 1–3 days post transfection (dpt) to visualize the continued survival of transfected cells. Phase images are from single planes near the center of the granuloma. tdTomato and *M. marinum* images are maximum projections of 70 μm z-stacks. (a,b) Similar results were observed in 3 independent experiments. Scale bars – 50 μm.

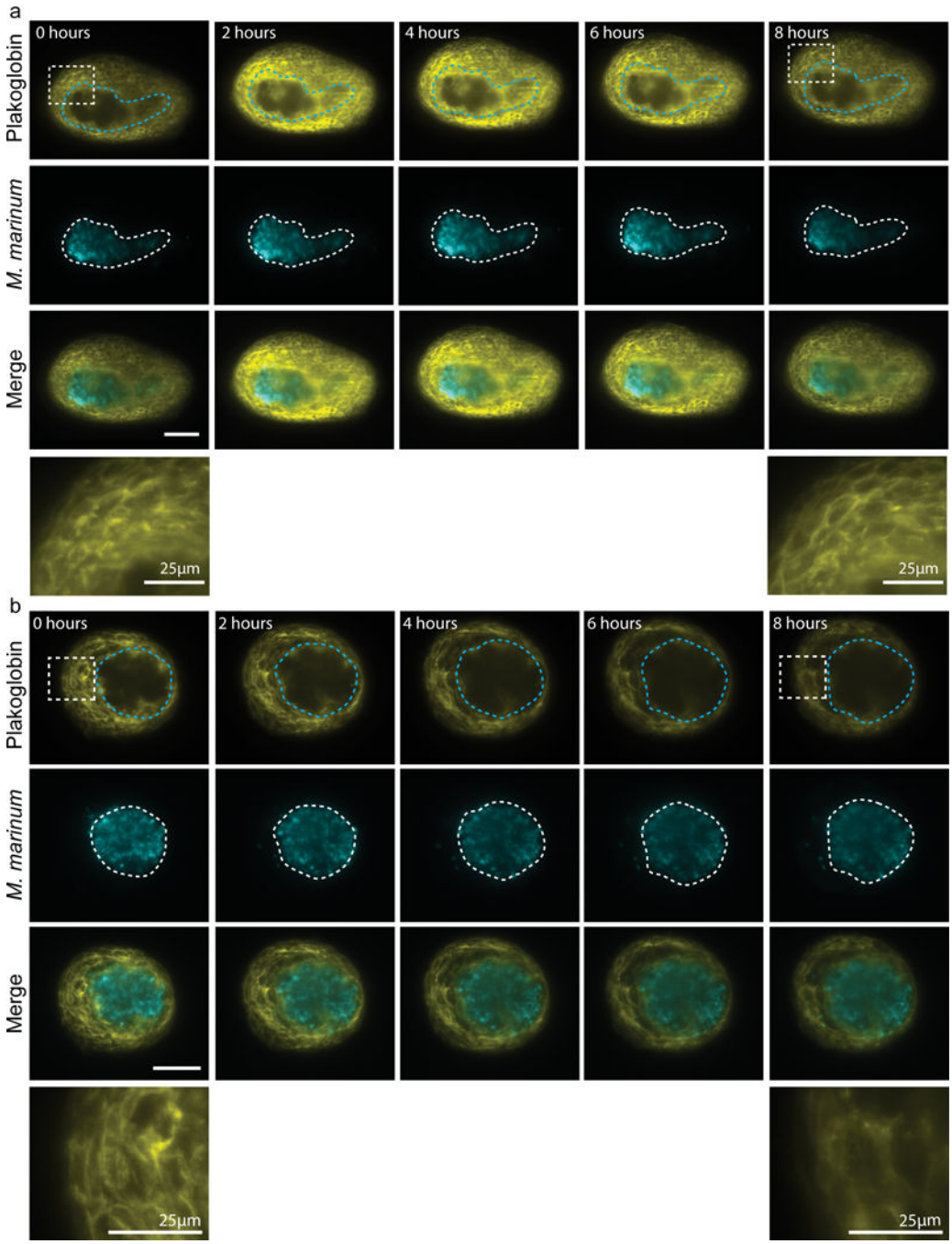


**Figure 6.**

PKC activity is required for adherens junction stability in mature granulomas. Granulomas were isolated from plakoglobin-citrine (yellow) gene trap animals infected with fluorescent *M. marinum* (cyan). Granulomas were treated with either (a) DMSO vehicle or (b) 10 μM Gö6983, embedded in agarose, and longitudinally imaged by lightsheet microscopy. Times on images indicate times post-treatment. Dotted cyan and white lines indicate the extent of the necrotic core. Dashed boxes in white denote areas that are enlarged in inset panels below. Images are maximum projections of a 6 μm z-stack from the center of the granuloma. Scale

bars – 50 μm, images of granulomas, 25 μm in inset panels. (a,b) PKC treatment was repeated 3 times with similar results.